KEK Preprint 92-196
February 1993
A

Resistive Wall Impedance of Beam Pipes of General Cross Section

Kaoru YOKOYA

Submitted to Particle Accelerators.

National Laboratory for High Energy Physics, 1993

KEK Reports are available from:

Technical Information & Library
National Laboratory for High Energy Physics
1-1 Oho, Tsukuba-shi
Ibaraki-ken, 305
JAPAN

Phone: 0298-64-1171
Telex: 3652-534 (Domestic)
(0)3652-534 (International)
Fax: 0298-64-4604
Cable: KEKOHO

RESISTIVE WALL IMPEDANCE OF BEAM PIPES OF GENERAL CROSS SECTION

Kaoru Yokoya

National Laboratory for High Energy Physics, Oho, Tsukuba-shi, Ibaraki, 305, Japan

Abstract

A method of calculating the coupling impedance and the wake function of resistive beam pipes is given including the short-range behavior of the wake. The pipe is uniform longitudinally but the cross section is arbitrary. The beam is assumed to be ultra-relativistic. A simple computer code is written using the boundary element method. Some results for elliptic, rectangular and hyperbolic pipes are presented.

Submitted to Particle Accelerators

keywords: coupling impedance, resistive wall

1 Introduction

The resistive wall impedance has been a topic in accelerator physics since 1960's and is thought to be well known but, in fact, it calls for further investigation still now. For example, in the future linear colliders, it causes some limitation of the machine design where the beam pipe is very close to the tiny beam such as in the collimators to scrape out the beam halo and in the final quadrupole magnets [1]. In these cases there is a possibility that we adopt beam pipes which are not round. The resistive wall impedance of non-axisymmetric structures has not yet been fully investigated. Up to now, the only wall shapes for which the exact solution is known including an arbitrary wave number and arbitrary locations of particles are the round pipe and two parallel plates [2,3,4,5].

Recently, Gluckstern, van Zeijts and Zotter [6] (GZZ) have derived formulas of longitudinal and transverse impedances for pipes with general cross section by using a beautiful formalism. Their resulting formulas are expressed as integrals of a function over the circumference of the cross section. This function is the tangential magnetic field on the wall in the absence of resistivity. Therefore, the formulas can easily be evaluated once the Laplace equation is solved analytically or numerically.

In this note, we are aiming some more advance in the following three points.

Firstly, although GZZ give the analytic solutions for the elliptic and rectangular cross-sections using their general formulas, we still need computers for other shapes in order to evaluate the formulas. We shall give a computer algorithm and some results for various shapes in this note.

Secondly, GZZ formula for the transverse impedance applies when the source particle (a dipole charge) and the witness particle are both on the axis (mirror symmetry of the pipe is assumed). Acutally, however, we need information for more geneal cases. The Lorentz force $\boldsymbol{F}$ on the witness particle is a function of the transverse position of the source particle $\boldsymbol{r}_s = (x_s, y_s)$ and of the witness particle $\boldsymbol{r}_w = (x_w, y_w)$ itself. For example, if the wall shape has mirror symmetries w.r.t. the x and y axes and $\boldsymbol{r}_s$ and $\boldsymbol{r}_w$ are small, linear terms will suffice. The vertical force is then $F_y = c_1 y_s + c_2 y_w$. The factor c_1 is usually called transverse impedance. The GZZ formula refers to this coefficient. In the case of a round pipe, c_2 vanishes because of the azimuthal symmetry. In general, however, this is not true. In fact, GZZ give this term analytically for the elliptic and rectangular pipes (they call this term 'incoherent') but general formulas for this term are not given. If the pipe is not round, c_2 is usually comparable to c_1 in magnitude.

This term c_2 can play a role in some cases. For example, consider the collimator problem. Usually, collimators are designed such that the kick angle by the c_1 term is smaller than the beam divergence angle when $\boldsymbol{r}_s$ is comparable to the beam size. This is enough for round pipes, because we need not take into account the source particles (bulk of the beam) far from the axis. However, if the pipe is not round, the c_2 term can be very large because we need to scrape large amplitude particles (large y_w).

Our computer code can compute the longitudinal and transverse forces for arbitrary locations of particles.

Thirdly, the formulas by GZZ apply only in the asymptotic region

$$\rho_0/L^2 \ll k \ll (L^2\rho_0)^{-1/3}, \qquad \text{or} \qquad L^2/\rho_0 \gg z \gg (L^2\rho_0)^{1/3}. \tag{1.1}$$

Here k is the wave number, z the distance between the source and witness particles, L the typical dimension of the wall crosssection. The parameter ρ_0, having the dimension of length, is defined by

$$\rho_0 = \frac{1}{\mu_0 c\sigma}, \tag{1.2}$$

where μ_0 is the permeability of vacuum and σ the conductivity of the wall material. ($\rho_0 \approx 0.5\times 10^{-10}$m for copper at room temparature.) In the region where these inequalities are satisfied, the wake function is a simple power of z ($z^{-3/2}$ for the longitudinal wake and $z^{-1/2}$ for the transverse.)

The first inequality sign in each expression in eq.(1.1) comes from δ_{skin}(skin depth) $\ll L$. (When the wall material is thin, L must be understood as the thickness of the material.) The physical meaning of the second inequality sign was clearly explained by K. Bane [3]. The finite conductivity slightly reduces the phase velocity, which is otherwise larger than the speed of light, so that the wave can couple to the beam, resulting a low-Q resonance. The latter inequality is not very important in applications so far, but it can play a role in the near future for very short bunches. For example, in recent designs of the final focus quad for linear colliders, the aperture is of order of 1cm. Then, the scale length is $(L^2\rho_0)^{1/3} \sim 20\mu$m, which is not extremely small compared with the typical bunch length 100μm. Moreover, a significant deviation from the simple power low actually starts at several times the scale length defined above. Therefore, we are already near the marginal point.

Our algorithm allows to compute such a short-range wake but, because of this problem, it is much more complicated than that in GZZ.

We will derive formulas of the impedance and the wake function in the next section. Sec. 3 discusses the method of numerical computation. The code is applied to pipes with various shapes and the results are described in Sec. 4.

2 Derivation of Impedance Formula

Assumptions and notation

We assume throughout that the pipe is uniform longitudinally and the beam is ultra-relativistic. The z-axis is parallel to the pipe. In the (x,y) plane, the vacuum region surrounded by the wall is denoted by Ω. The coordinate s is the length measured along the wall surface $\partial\Omega$. The unit normal (outward from Ω) and tangential vectors at s are denoted by $\boldsymbol{n}(s)$ and $\boldsymbol{\tau}(s)$, respectively, and the unit vector along z by $\boldsymbol{e}_z$. The three vectors $\boldsymbol{n}$, $\boldsymbol{\tau}$ and $\boldsymbol{e}_z$ form a right-handed basis. The source and the witness charge (unit charge) are located at $\boldsymbol{r}_s = (x_s, y_s)$ and $\boldsymbol{r}_w = (x_w, y_w)$, respectively.

We work in the frequency domain and define the Fourier transform of any function of time $f(t)$ by $\int f(t)e^{i\omega t}dt$ (without the factor $1/2\pi$). All the field quantities which are effective on the wake field are proportional to $\exp i(kz-\omega t)$ ($k=\omega/c$) because of the longitudinal uniformity. Our definitions of the fields do not include this factor. Thus, to go to the time domain, one need to multiply $ce^{ik(z-ct)}/2\pi$ and to integrate over k. We assume k is positive. Formulas for negative k can easily be obtained because the physical quantities are real.

We write the electric and magnetic fields as $\boldsymbol{E}+\boldsymbol{E}^{(0)}$ and $\boldsymbol{H}+\boldsymbol{H}^{(0)}$, where the superscript (0) denotes solutions in the case of the perfectly conducting wall with the same wall shape. One can easily show that the transverse Lorentz force $\boldsymbol{F}_\perp=\boldsymbol{E}_\perp+Z_0\boldsymbol{e}_z\times\boldsymbol{H}$ (the subscript $\perp$ denotes the component perpendicular to $\boldsymbol{e}_z$) satisfies

$$\boldsymbol{F}_\perp=\frac{1}{ik}\nabla_\perp E_z, \tag{2.3}$$

where $\nabla_\perp$ is the two-dimensional gradient. Therefore, all the needed information is obtained from E_z, since $\boldsymbol{E}^{(0)}$ and $\boldsymbol{H}^{(0)}$ do not contribute to the wake function.

Kirchhoff integral formula

Since $(\boldsymbol{E},\boldsymbol{H})$ obeys the sourceless Maxwell equation, it satisfies the (vector version of the) Kirchhoff integral formula (see, for example,[7]). In our case where the field is proportional to $e^{ik(z-ct)}$, the formula can be written as

$$E_z(\boldsymbol{r})=\oint ds'\left[-ik(Z_0H_\tau-E_n)G(\boldsymbol{r},\boldsymbol{r}')-E_z\boldsymbol{n}'\cdot\nabla'_\perp G(\boldsymbol{r},\boldsymbol{r}')\right], \tag{2.4}$$

$$\boldsymbol{E}_\perp(\boldsymbol{r})=\oint ds'\left[-ik(\boldsymbol{n}'E_z-\boldsymbol{\tau}'Z_0H_z)G(\boldsymbol{r},\boldsymbol{r}')-E_n\nabla'_\perp G(\boldsymbol{r},\boldsymbol{r}')-E_\tau\boldsymbol{e}_z\times\nabla'_\perp G(\boldsymbol{r},\boldsymbol{r}')\right], \quad (\boldsymbol{r}\in\Omega). \tag{2.5}$$

Here, $\oint$ is the integral along $\partial\Omega$ and the prime refers to the quantities evaluated on the wall at s'. (We omit the primes for the field variables on the right-hand side.) The function G is the Green function satisfying

$$\Delta_\perp G(\boldsymbol{r},\boldsymbol{r}')=-\delta(\boldsymbol{r}-\boldsymbol{r}'). \tag{2.6}$$

The Kirchhoff formula is valid for any Green function satisfying this equation but for simplicity we choose the solution in the free space;

$$G(\boldsymbol{r},\boldsymbol{r}')=-\frac{1}{2\pi}\log|\boldsymbol{r}-\boldsymbol{r}'|, \qquad \nabla'_\perp G(\boldsymbol{r},\boldsymbol{r}')=\frac{1}{2\pi}\frac{\boldsymbol{r}-\boldsymbol{r}'}{|\boldsymbol{r}-\boldsymbol{r}'|^2}. \tag{2.7}$$

By taking the limit that $\boldsymbol{r}$ approaches the wall surface $\partial\Omega$ (from inside Ω), we obtain integral equations where only the fields on the wall appear. Let us define following operators which transform functions on $\partial\Omega$.

$$(\mathcal{D}f)(s)=\oint ds'(\boldsymbol{n}'\cdot\nabla'_\perp G)f(s')+f(s), \tag{2.8}$$

$$(\mathcal{G}f)(s) = \oint ds' G(\boldsymbol{r}, \boldsymbol{r}') f(s'), \tag{2.9}$$

$$(\mathcal{N}f)(s) = \oint ds' (\boldsymbol{n} \cdot \nabla'_\perp G) f(s') + f(s), \tag{2.10}$$

$$(\mathcal{T}f)(s) = \oint ds' (\boldsymbol{\tau} \cdot \nabla'_\perp G) f(s'), \tag{2.11}$$

$$(\mathcal{C}f)(s) = \oint ds' (\boldsymbol{n} \cdot \boldsymbol{n}') G(\boldsymbol{r}, \boldsymbol{r}') f(s') = \oint ds' (\boldsymbol{\tau} \cdot \boldsymbol{\tau}') G(\boldsymbol{r}, \boldsymbol{r}') f(s'), \tag{2.12}$$

$$(\mathcal{S}f)(s) = \oint ds' (\boldsymbol{\tau} \cdot \boldsymbol{n}') G(\boldsymbol{r}, \boldsymbol{r}') f(s') = -\oint ds' (\boldsymbol{n} \cdot \boldsymbol{\tau}') G(\boldsymbol{r}, \boldsymbol{r}') f(s'). \tag{2.13}$$

Here, rigorously speaking, $\boldsymbol{r}$ on the right-hand side must be replaced by $\boldsymbol{r}(s) - \epsilon \boldsymbol{n}(s)$ and the limit $\epsilon \longrightarrow 0_+$ must be taken. Then, from eqs.(2.4) and (2.5) we obtain integral equations

$$\mathcal{D} \left| E_z \right\rangle = -ik\mathcal{G} \left| Z_0 H_\tau - E_n \right\rangle, \tag{2.14}$$

$$\mathcal{N} \left| E_n \right\rangle - \mathcal{T} \left| E_\tau \right\rangle = -ik \left[\mathcal{C} \left| E_z \right\rangle + \mathcal{S} \left| Z_0 H_z \right\rangle \right], \tag{2.15}$$

$$\mathcal{T} \left| E_n \right\rangle + \mathcal{N} \left| E_\tau \right\rangle = -ik \left[\mathcal{S} \left| E_z \right\rangle - \mathcal{C} \left| Z_0 H_z \right\rangle \right]. \tag{2.16}$$

For notational convenience, we have introduced the 'ket' vector $|\ \rangle$ to denote a function on $\partial\Omega$.

Approximate boundary condition

In order to solve eqs. (2.14), (2.15) and (2.16), we need the boundary conditions on the wall surface. Under the assumption that the skin depth δ_{skin} is much smaller than L, the typical dimension of Ω, (and than the thickness of the wall material), the resistivity effect can be expressed by approximate boundary conditions.

Within the wall material, the Maxell equation for the field having the (z,t) dependence $\exp[ik(z-ct)]$ can be written in the form (for a while, we shall denote the total field by $\boldsymbol{E}$ and $\boldsymbol{H}$)

$$\Delta_\perp \boldsymbol{E} + \kappa^2 \boldsymbol{E} = 0, \qquad \nabla_\perp \cdot \boldsymbol{E}_\perp + ikE_z = 0, \tag{2.17}$$

and

$$Z_0 \boldsymbol{H} = \frac{1}{ik} (\nabla_\perp + ik\boldsymbol{e}_z) \times \boldsymbol{E}, \tag{2.18}$$

with

$$\kappa \equiv e^{\pi i/4} \sqrt{\mu_0 ck\sigma} = \frac{1+i}{\delta_{skin}} = e^{\pi i/4} \sqrt{\frac{k}{\rho_0}}, \qquad \delta_{skin} = \sqrt{\frac{2}{\mu_0 ck\sigma}}, \tag{2.19}$$

where ρ_0 has already been defined in eq.(1.2).

Solutions to the equation for $\boldsymbol{E}$ are in general linear combinations of the form

$$\boldsymbol{E}(\boldsymbol{r}) = \boldsymbol{E}_0 e^{i\kappa \boldsymbol{\alpha} \cdot \boldsymbol{r}}, \tag{2.20}$$

where $\boldsymbol{\alpha}$ is a unit vector in the (x,y) plane and $\boldsymbol{E}_0$ is a constant satisfying

$$(\kappa \boldsymbol{\alpha} + k\boldsymbol{e}_z) \cdot \boldsymbol{E}_0 = 0. \tag{2.21}$$

Consider the field in the vacuum region near the boundary. The field expressed by eq.(2.20) has a very rapid variation along the wall surface with the typical scale length δ_{skin} unless $\boldsymbol{\alpha}$ is almost parallel to $\boldsymbol{n}$. In the vacuum region, the typical length of field variation is the wavelength $\lambda = 1/k$ or the curvature radius of the surface, the latter being represented by L. (Rigorously speaking, this is not true if the wall has a cusp, where the curvature radius is infinitesimally small.) Therefore, so long as $\delta_{skin} \ll \lambda$ and $\delta_{skin} \ll L$, $\boldsymbol{\alpha} \approx \boldsymbol{n}$ holds approximately. The condition $\delta_{skin} \ll \lambda$ is equivalent to $\lambda \gg \rho_0$, which is never violated in practice. (In any case, we cannot trust Ohm's law down to such a small scale ρ_0.) Therefore, our basic assumption is $\delta_{skin} \ll L$ only.

From eq.(2.18), we obtain approximate boundary conditions

$$Z_0 H_\tau = -\frac{\kappa}{k} E_z, \qquad Z_0 H_z = \frac{\kappa}{k} E_\tau. \tag{2.22}$$

Note that the components appearing in these expressions are continuous across the boundary. Nothing can be said about the normal component under our assumption $\delta_{skin} \ll L$. Returning to the original notation where the field is expressed like $\boldsymbol{E} + \boldsymbol{E}^{(0)}$, we write the boundary conditions as

$$Z_0(H_\tau + H_\tau^{(0)}) = -\frac{\kappa}{k} E_z, \tag{2.23}$$

$$Z_0 H_z = \frac{\kappa}{k} E_\tau. \tag{2.24}$$

(Note that the longitudinal fields and the tangential electric field are zero in the case of perfectly conducting walls.) The term H_τ in eq.(2.23) is ignored in GZZ. When the resistivity is sufficiently small, we can treat it as a perturbation. The wall current, which is proportional to $H_\tau^{(0)}$, causes a longitudinal electric field E_z due to the resistivity. According to Ampére's law $\nabla \times Z_0 \boldsymbol{H} = -ik\boldsymbol{E}$, E_z generates a magnetic field. $Z_0 H_\tau$ created in this way is of the order of $L \times kE_z \sim Lk \times (k/\kappa) Z_0 H_\tau^{(0)} \sim k^2 L \delta_{skin} Z_0 H_\tau^{(0)}$. Therefore, only when $k^2 L \delta_{skin} \ll 1$, the perturbation treatment is justified. This is the condition (1.1) (upper bound of k) mentioned in the introduction.

Solving the integral equation

Now, let us return to the integral equations (2.14), (2.15) and (2.16). Replacing H_z in eqs.(2.15) and (2.16) with eq.(2.24), we can eliminate E_τ and express E_n in terms of E_z. Then, substituting the resulting expression into eq.(2.14) and using the other boundary condition (2.23), we get an integral equation for E_z.

Let us compare the magnitude of each term appearing in eqs.(2.15) and (2.16). Since the typical scale of the operators $\mathcal{C}$ and $\mathcal{S}$ is the typical wall dimension L, the term with H_z in eqs.(2.15) and (2.16) is $\sim kL(\kappa/k)E_\tau \sim (L/\delta_{skin})E_\tau$, while the second term in the left-hand side is $\sim E_\tau$ because the operators $\mathcal{N}$ and $\mathcal{T}$ are of order unity. Therefore, we can ignore the E_τ terms on the left-hand side. Then, eqs.(2.15) and (2.16) can formally be solved as

$$|E_n\rangle = -ik\mathcal{M}\,|E_z\rangle\,, \tag{2.25}$$

where

$$\mathcal{M} = (\mathcal{N} + \mathcal{S}\mathcal{C}^{-1}\mathcal{T})^{-1}(\mathcal{C} + \mathcal{S}\mathcal{C}^{-1}\mathcal{S}). \tag{2.26}$$

(We assume the existence of the inverse operators.) Note that the boundary condition for H_z is not actually used except the fact that the coefficient κ/k is very large.

Now, let us solve eq.(2.14) with the boundary condition (2.23);

$$\mathcal{D}\,|E_z\rangle = ik\mathcal{G}\left|\frac{\kappa}{k}E_z + Z_0 H_\tau^{(0)} + E_n\right\rangle. \tag{2.27}$$

Since the operator $\mathcal{G}$ is $O(L)$, the left-hand side of this equation is smaller than the first term on the right-hand side by the factor $O(1/\kappa L) \sim O(\delta_{skin}/L)$ and, therefore, we can ignore the left-hand side. Thus, by using eq.(2.25), we obtain

$$|E_z\rangle = \frac{k}{\kappa}\left[1 - i\frac{k^2}{\kappa}\mathcal{M}\right]^{-1}\left|Z_0 H_\tau^{(0)}\right\rangle. \tag{2.28}$$

Thus, once the field for the perfectly conducting wall is given, we can get E_z on the wall surface.

Solution for the perfectly conducting case

Next, let us find the field for the case of the perfectly conducting wall. From the Maxwell equations, one can easily find that the longitudinal fields vanish $E_z^{(0)} = H_z^{(0)} = 0$ and the transverse electric field $\boldsymbol{E}_\perp^{(0)}$ satisfies

$$\boldsymbol{E}_\perp^{(0)} = -Z_0 \nabla_\perp \phi, \tag{2.29}$$

with

$$\Delta_\perp \phi = -\delta(\boldsymbol{r} - \boldsymbol{r}_s) \qquad \text{and} \qquad \phi = 0 \quad \text{(on the wall)}. \tag{2.30}$$

The transverse magnetic field is given by

$$Z_0 \boldsymbol{H}_\perp^{(0)} = \boldsymbol{e}_z \times \boldsymbol{E}_\perp^{(0)}. \tag{2.31}$$

We split ϕ into two parts g_s and ϕ_1, the former being the solution in the free space $g_s(\boldsymbol{r}) = G(\boldsymbol{r}, \boldsymbol{r}_s)$. Then, the latter obeys the sourceless Laplace equation with the boundary condition $\phi_1 = -g_s$ on the wall and, therefore, satisfies the Kirchhoff integral formula

$$\mathcal{D}\,|-g_s\rangle = \mathcal{G}\,|\partial\phi_1/\partial n\rangle\,. \tag{2.32}$$

Thus, we obtain

$$\left|Z_0 H_\tau^{(0)}\right\rangle = |E_n\rangle = -Z_0\,|\partial g_s/\partial n + \partial\phi_1/\partial n\rangle = Z_0\,|u\rangle\,, \tag{2.33}$$

where

$$|u\rangle = \mathcal{G}^{-1}\mathcal{D}\,|g_s\rangle - |\partial g_s/\partial n\rangle\,. \tag{2.34}$$

Thus, we have E_z on the wall as

$$|E_z\rangle = \frac{Z_0 k}{\kappa}\left[1 - i\frac{k^2}{\kappa}\mathcal{M}\right]^{-1}|u\rangle\,. \tag{2.35}$$

The field at the witness particle

To find E_z at the witness particle, we go back to the Kirchhoff formula (2.4), which can formally be written as

$$E_z(\boldsymbol{r}_w) = -ik\,\langle g_w|Z_0 H_\tau - E_n\rangle - \langle g'_w|E_z\rangle\,, \tag{2.36}$$

where g_w and g'_w are functions on $\partial\Omega$ defined by

$$g_w(s) = G(\boldsymbol{r}_w, \boldsymbol{r}) \qquad \text{and} \qquad g'_w = \partial g_w/\partial n = \boldsymbol{n}\cdot\nabla_\perp G(\boldsymbol{r}_w, \boldsymbol{r}). \tag{2.37}$$

The brakets $\langle\ |\ \rangle$ define the scalar product as an integral over the circumference of the crosssection;

$$\langle u|v\rangle \equiv \oint ds\, u^*(s)\, v(s), \tag{2.38}$$

where the asterisk denotes complex conjugate. Since the combination $Z_0 H_\tau - E_n$ satisfies eq.(2.14), we can rewrite eq.(2.36) in terms of E_z only as

$$E_z(\boldsymbol{r}_w) = \langle v|E_z\rangle\,, \tag{2.39}$$

where

$$\langle v| \equiv \langle g_w|\,\mathcal{G}^{-1}\mathcal{D} - \langle g'_w|\,, \qquad \text{or} \qquad |v\rangle = [\mathcal{G}^{-1}\mathcal{D}]^\dagger\,|g_w\rangle - |g'_w\rangle\,. \tag{2.40}$$

Here, the superscript $\dagger$ denotes the adjoint of an operator defined according to the scalar product (2.38), i.e, $\left\langle \mathcal{A}^\dagger u|v\right\rangle = \langle u|\mathcal{A}v\rangle$ for any functions u and v. In the above case, the superscript can be omitted because $\mathcal{G}^{-1}\mathcal{D}$ is self-adjoint (see Appendix. A).

Thus, finally we can write E_z at the witness particle in the form

$$E_z(\boldsymbol{r}_w) = Z_0\frac{k}{\kappa}\,\langle v|\left[1 - i\frac{k^2}{\kappa}\mathcal{M}\right]^{-1}|u\rangle\,. \tag{2.41}$$

Eigenvalues and eigenfunctions of the operator $\mathcal{M}$

Let us rewrite eq.(2.41) in a form more convenient for numerical calculations. As is proved in Appendix. A, the operator $\mathcal{M}$ is self-adjoint. Therefore, the eigenvalues are real. We denote the eigenvalue by μ_α and the eigenfunction by $|\alpha\rangle$, which is normalized as $\langle\alpha|\alpha\rangle = 1$. Then, eq.(2.41) can be written as

$$E_z(\boldsymbol{r}_w) = Z_0\frac{k}{\kappa}\sum_\alpha \frac{c_\alpha}{1 - i(k^2/\kappa)\mu_\alpha}, \tag{2.42}$$

where

$$c_\alpha(\boldsymbol{r}_w, \boldsymbol{r}_s) = \langle v|\alpha\rangle\,\langle\alpha|u\rangle\,. \tag{2.43}$$

The transverse force is then given, using eq.(2.3), by

$$\boldsymbol{F}_\perp(\boldsymbol{r}_w) = -i\frac{Z_0}{\kappa}\sum_\alpha \frac{\partial c_\alpha/\partial \boldsymbol{r}_w}{1-i(k^2/\kappa)\mu_\alpha}, \tag{2.44}$$

where the coefficients $\partial c_\alpha/\partial \boldsymbol{r}_w$ can be calculated simply by using $\partial g_w/\partial \boldsymbol{r}_w$ instead of g_w in eq.(2.37).

A nice feature of these expressions (2.42) and (2.44) is that the dependences on the location of the source and the witness particles are all confined in the function u and v, respectively. The most time-consuming part is the diagonalization of $\mathcal{M}$, which depends on the shape of the wall but does not depend on $\boldsymbol{r}_s$ and $\boldsymbol{r}_w$, nor on the wave number k.

Asymptotic form for $k \ll (L^2\rho_0)^{-1/3}$

Because μ_α =O(L) and, therefore, $(k^2/\kappa)\mu_\alpha$ = O($k^{3/2}\rho_0^{1/2}L$), one can ignore the term with μ_α in the denominator of eq.(2.42) in the asymptotic region $k \ll (L^2\rho_0)^{-1/3}$. Since the sum $|\alpha\rangle\langle\alpha|$ over all the eigenfunctions is identity, we get

$$E_z = Z_0\frac{k}{\kappa}\langle v|u\rangle = Z_0\frac{k}{\kappa}\oint ds\, v^*(s)u(s), \qquad (k \ll (L^2\rho_0)^{-1/3}). \tag{2.45}$$

When $\boldsymbol{r}_s = \boldsymbol{r}_w$, we have $u = v$ and, consequently,

$$E_z = Z_0\frac{k}{\kappa}\oint ds\, |u(s)|^2, \qquad (k \ll (L^2\rho_0)^{-1/3}, \boldsymbol{r}_s = \boldsymbol{r}_w) \tag{2.46}$$

which is equivalent to the longitudinal impedance formula obtained by GZZ. Thus, if one is interested only in the asymptotic form, the operator $\mathcal{M}$ is not needed.

The asymptotic form for the transverse force is

$$\boldsymbol{F}_\perp(\boldsymbol{r}_w) = -i\frac{Z_0}{\kappa}\oint ds\, \frac{\partial v^*(s)}{\partial \boldsymbol{r}_w}u(s), \qquad (k \ll (L^2\rho_0)^{-1/3}). \tag{2.47}$$

Usual definition of the transverse impedance (per unit displacement of the source particle per unit pipe length) is equivalent to $Z_y = \partial F_y/\partial y_s$ (vertical impedance). Thus, for $\boldsymbol{r}_s = \boldsymbol{r}_w$, we obtain

$$Z_y = -i\frac{Z_0}{\kappa}\oint ds\, \left|\frac{\partial u}{\partial y_s}\right|^2, \qquad (k \ll (L^2\rho_0)^{-1/3}, \boldsymbol{r}_s = \boldsymbol{r}_w), \tag{2.48}$$

which again agrees with the transverse impedance formula of GZZ.

Wake function

Since all the terms in eqs.(2.42) and (2.44) have the same wavenumber dependence, the wake function can easily be computed from two basic functions f_L and f_T defined

in Appendix. B;

$$W_L(z) \equiv \frac{1}{2\pi}\int_{-\infty}^{+\infty} E_z(k)e^{-ikz}cdk = \sum_\alpha \frac{cZ_0}{\mu_\alpha}c_\alpha f_L(z/z_\alpha), \tag{2.49}$$

$$\boldsymbol{W}_\perp(z) \equiv \frac{1}{2\pi}\int_{-\infty}^{+\infty} \boldsymbol{F}_\perp(k)e^{-ikz}cdk = \sum_\alpha \frac{cZ_0 z_\alpha}{\mu_\alpha}\frac{\partial c_\alpha}{\partial \boldsymbol{r}_w} f_T(z/z_\alpha), \tag{2.50}$$

where

$$z_\alpha = [(2\mu_\alpha)^2\rho_0]^{1/3}. \tag{2.51}$$

(The sign of W_L is chosen such that the accecelaration is positive. Also note that the transverse impedance in the usual definition is $\partial W_x/\partial x_s$ and $\partial W_y/\partial y_s$.) The asymptotic forms for large $z \gg (L^2\rho_0)^{1/3}$ are found to be

$$W_L(z) \approx \frac{cZ_0\sqrt{\rho_0}}{2\sqrt{\pi}z^{3/2}}\sum_\alpha c_\alpha = \frac{cZ_0\sqrt{\rho_0}}{2\sqrt{\pi}z^{3/2}}\langle v|u\rangle, \tag{2.52}$$

$$\boldsymbol{W}_\perp(z) \approx \frac{cZ_0\sqrt{\rho_0}}{\sqrt{\pi}\sqrt{z}}\sum_\alpha \frac{\partial c_\alpha}{\partial \boldsymbol{r}_w} = \frac{cZ_0\sqrt{\rho_0}}{\sqrt{\pi}\sqrt{z}}\left\langle \frac{\partial v}{\partial \boldsymbol{r}_w}|u\right\rangle, \tag{2.53}$$

using the asymtotic forms for f_L and f_T given in Appendix. B.

The Ohmic loss

The energy dissipated in a unit volume in the wall material by a point charge at $\boldsymbol{r}_s$ is given by

$$\frac{c\sigma}{2\pi}\int_{-\infty}^{\infty} dk\,|\boldsymbol{E}|^2. \tag{2.54}$$

Since the field in the material can be approximated by eq.(2.20) with $\alpha \approx \boldsymbol{n}$, we obtain the energy loss per unit pipe length by integrating over the normal direction and over the circumference as

$$-\frac{d\mathcal{E}}{dz} = \frac{c\sigma}{2\pi}\int_{-\infty}^{\infty} dk \oint ds \frac{\delta_{skin}}{2}|\boldsymbol{E}_0(k,s)|^2. \tag{2.55}$$

Note that $\boldsymbol{E}_0$ is the field on the wall just outside $\partial\Omega$. From the condition (2.21), we find $E_n/E_z = O(\delta_{skin}/\lambda)$. Since E_τ and E_z are continuous across $\partial\Omega$, we may use the values in Ω. From the fact that H_z/E_z=$O(1)$, which can be obtained by eqs.(2.15) and (2.16), and from eq.(2.24), we find that E_τ/E_z=$O(\delta_{skin}/\lambda)$. Thus, we may ignore E_n and E_τ in $|\boldsymbol{E}_0|$ in eq.(2.55) and replace it by $|E_z|$. By using eq.(2.35) and the eigenvalues of $\mathcal{M}$, we get

$$\oint ds\,|E_z|^2 = \langle E_z|E_z\rangle = Z_0^2 k\rho_0 \sum_\alpha \langle u|\alpha\rangle \left|1 - e^{\pi i/4}k^{3/2}\rho_0^{1/2}\mu_\alpha\right|^{-2}\langle\alpha|u\rangle. \tag{2.56}$$

The integration over k can be performed analytically with the result

$$-\frac{d\mathcal{E}}{dz} = \frac{cZ_0}{2}\sum_\alpha \frac{c_\alpha(\boldsymbol{r}_s,\boldsymbol{r}_s)}{\mu_\alpha}, \tag{2.57}$$

where c_α is defined in eq.(2.43) but is to be evaluated for $\boldsymbol{r}_w = \boldsymbol{r}_s$, or, $v = u$. From eq.(2.49) with the normalization $f_L(0_+) = -1$, we can reproduce the well-known formula of the loss factor

$$k_L(0) = -\frac{d\mathcal{E}}{dz} = -\frac{1}{2}W_L(0_+). \tag{2.58}$$

When the source charge is not a point but has a finite length, we need to multiply the Fourier spectrum of the charge distribution, which is $e^{-k^2\sigma_z^2}$ in the case of Gaussian distribution with the r.m.s. length σ_z. The loss parameter is given by

$$k_L(\sigma_z) = -\int_0^\infty W_L(z)\frac{1}{\sqrt{4\pi}\sigma_z}e^{-z^2/4\sigma_z^2}dz = \sum_\alpha \frac{cZ_0c_\alpha(\boldsymbol{r}_s, \boldsymbol{r}_s)}{2\mu_\alpha}g_L(\sigma_z/z_\alpha), \tag{2.59}$$

where the function g_L is defined in Appendix. B. The asymptotic form for long bunches is

$$k_L(\sigma_z) \approx \frac{\Gamma(3/4)}{2\sqrt{2}\pi}\frac{cZ_0\sqrt{\rho_0}}{\sigma_z^{3/2}}\sum_\alpha c_\alpha. \tag{2.60}$$

The AC Conductivity at High Frequencies

As pointed out by Bane [3], the AC conductivity is nolonger equal to the DC conductivity at very high frequencies and is approximately expressed by $\sigma/(1 - i\omega\tau)$, τ being the relaxation time of the metal. Our formulas in the frequency domain are still valid in such a case. The wake function, however, cannot be expressed by the two functions $f_L(\zeta)$ and $f_T(\zeta)$. We need one more parameter related to the relaxation time τ. Thus, $f_L(z/z_\alpha)$ and $f_T(z/z_\alpha)$ in eqs.(2.49) and (2.50) have to be replaced with two-argument functions $f_L(z/z_\alpha, c\tau/z_\alpha)$ and $f_T(z/z_\alpha, c\tau/z_\alpha)$ defined in Appendix. B. Since the AC conductivity effect plays a role only at high frequencies, the asymptotic forms of the wake functions (2.52) and (2.53) remain unchanged but, of course, the condition $z \gg c\tau$ is needed in addition to $z \gg (L^2\rho_0)^{1/3}$.

3 Numerical Methods

The formulas given in the previous section can easily be coded. What is needed is to express all the operators in the form of matrices, by discretizing the wall shape and the functions. Select N points (nodes) on the wall and denote their s coordinate by s_i (i=1,2,...N). The simplest way of discretization is to approximate a function $f(s)$ by a piece-wise constant function:

$$f(s) \approx \sum_{i=1}^{N} f_i\rho_i(s), \tag{3.61}$$

with

$$\rho_i(s) = \begin{cases} 1/\sqrt{l_i} & (s_i < s < s_{i+1}) \\ 0 & (\text{else}) \end{cases}, \tag{3.62}$$

where $l_i = s_{i+1} - s_i$ is the length of the i-th segment. The normalization of ρ_i is chosen such that the norm of f is given by

$$\langle f|f\rangle = \oint ds\,|f(s)|^2 = \sum_i |f_i|^2 . \tag{3.63}$$

Thus, the approximate value of $f(s)$ on the i-th segment is not f_i but $f_i/\sqrt{l_i}$.

Let us denote the operator defined by a kernel $K(s,s')$ by $\mathcal{K}$; i.e., the operator form

$$|g\rangle = \mathcal{K}\,|f\rangle \tag{3.64}$$

corresponds to the integral form

$$g(s) = \oint ds K(s,s') f(s'). \tag{3.65}$$

Let us suppose that $f(s)$ and $g(s)$ are approximately expressed by f_i and g_i. Multiplying eq.(3.65) by $\rho_i(s)$ and integrating over s, we obtain the corresponding matrix form

$$g_i = \sum_{i=1}^{N} K_{i,j} f_j, \tag{3.66}$$

with

$$K_{i,j} = \frac{1}{\sqrt{l_i l_j}} \int_{s_i}^{s_{i+1}} ds \int_{s_j}^{s_{j+1}} ds' K(s,s'). \tag{3.67}$$

We must carefully treat the kernel of the operators $\mathcal{D}$, $\mathcal{N}$ and $\mathcal{T}$ because of their strong singularity near $s = s'$. The definition (2.8) of the operator $\mathcal{D}$ must be understood as the limit of the field point approaching the wall from inside Ω, i.e.,

$$(\mathcal{D}f)(s) = f(s) + \lim_{\epsilon\to 0+} \oint ds' \boldsymbol{n}(s') \cdot [\nabla'_\perp G(\boldsymbol{r}, \boldsymbol{r}(s'))]_{\boldsymbol{r}=\boldsymbol{r}(s)-\epsilon\boldsymbol{n}(s)} f(s') \tag{3.68}$$

where $\boldsymbol{r}(s)$ denotes the point on the wall. If the wall is smooth at the point s, the limit can be expressed in the form

$$(\mathcal{D}f)(s) = \frac{1}{2} f(s) + \mathrm{pv} \oint ds' \boldsymbol{n}(s') \cdot \nabla'_\perp G(\boldsymbol{r}(s), \boldsymbol{r}(s')) f(s'), \tag{3.69}$$

where pv denotes Cauchy's principal value. The same expression holds for $\mathcal{N}$ with $\boldsymbol{n}(s')$ replaced with $\boldsymbol{n}(s)$. For the definition (2.11) of $\mathcal{T}$ we only need to take the principal value.

To perform the integration in eq.(3.67), we need the boundary shape between s_i and s_{i+1}. The simplest choice is the straight line but we use the cubic spline interpolation for better accuracy.

Thus, we can now express the operators $\mathcal{G}$, $\mathcal{D}$, $\mathcal{N}$, $\mathcal{T}$, $\mathcal{C}$ and $\mathcal{S}$ in matrix forms. The resulting matrices have the symmetry

$$G_{i,j} = G_{j,i}, \quad C_{i,j} = C_{j,i}, \quad S_{i,j} = -S_{j,i}, \quad D_{i,j} + N_{j,i} = \delta_{i,j}. \tag{3.70}$$

These relations are exactly satisfied with a finite number of nodes N owing to the prescription (3.67). Unfortunately, however, the symmetries of the matrices corresponding to the operators $\mathcal{G}^{-1}\mathcal{D}$ and $\mathcal{M}$, whose elements are computed not from explicit kernels but from matrix manipulations, are violated by $O(1/N)$.

4 Applications

Round pipe

Let us first illustrate our formalism for a round pipe. In this case everything can be done analytically.

The kernels of all the operators depend only on $s-s'$, or, equivalently, $\theta-\theta'$, where θ is the azimuthal angle in the (x,y) plane. Also, they are periodic in $\theta-\theta'$. Therefore, the eigenfunctions have the form $|m\rangle = e^{im\theta}/\sqrt{2\pi a}$ (m=0,±1,±2,...). One can compute the eigenvalues analytically with the result

$$\mu_m = \begin{cases} a/2 & (m=0) \\ a/(|m|+1) & (m \neq 0), \end{cases} \tag{4.71}$$

where a is the pipe radius. One finds that the three modes m=0 and ±1 are degenerate.

Let the source particle be on the x-axis and denote the location of the witness particle by the polar coordinate r_w and θ_w. The functions u and v are found easily as

$$u(\theta) = \frac{1}{2\pi a}\frac{a^2-x_s^2}{a^2+x_s^2-2ax_s\cos\theta} = \frac{1}{2\pi a}\sum_{m=-\infty}^{\infty}\left(\frac{x_s}{a}\right)^{|m|}e^{im\theta}, \tag{4.72}$$

$$v(\theta) = \frac{1}{2\pi a}\frac{a^2-r_w^2}{a^2+r_w^2-2ar_w\cos(\theta-\theta_w)} = \frac{1}{2\pi a}\sum_{m=-\infty}^{\infty}\left(\frac{r_w}{a}\right)^{|m|}e^{im(\theta-\theta_w)}, \tag{4.73}$$

and the coefficient c_m can be written as

$$c_m = \frac{1}{2\pi a}e^{im\theta_w}\left(\frac{r_w}{a}\right)^{|m|}\left(\frac{x_s}{a}\right)^{|m|}. \tag{4.74}$$

Thus, we reproduce the well-known formula

$$E_z = \frac{Z_0 k}{2\pi a\kappa}\sum_{m=-\infty}^{\infty}\frac{1}{1-i\mu_m k^2/\kappa}e^{im\theta_w}\left(\frac{r_w}{a}\right)^{|m|}\left(\frac{x_s}{a}\right)^{|m|}. \tag{4.75}$$

We find our mode classification as the eigenmode of the operator $\mathcal{M}$ is identical to the azimuthal mode in the case of the round pipe. When the particles are at the origin $\boldsymbol{r}_s = \boldsymbol{r}_w = 0$, $u(s)$ and $v(s)$ are constant and consequently only the mode $m = 0$ contributes. When $\boldsymbol{r}_s$ is small, only the modes $m = \pm 1$ contribute to the transverse impedance $\partial E_z/\partial \boldsymbol{r}_w$.

Eigenmodes and eigenvalues

Next, let us discuss the modes for elliptic pipes with the horizontal radius a and vertical b ($a > b$). In this case, the modes can be labeled by the number of nodes of the eigenfunction, which is, of course, even. We denote half the number of nodes by m. An example of the eigenfunction is plotted in Fig. 1. For each $m \geq 1$, there are two modes, one even in x and odd in y ($\sin m\theta$-like) and the other odd in x and even in y ($\cos m\theta$-like). The former has the larger eigenvalue if $a > b$.

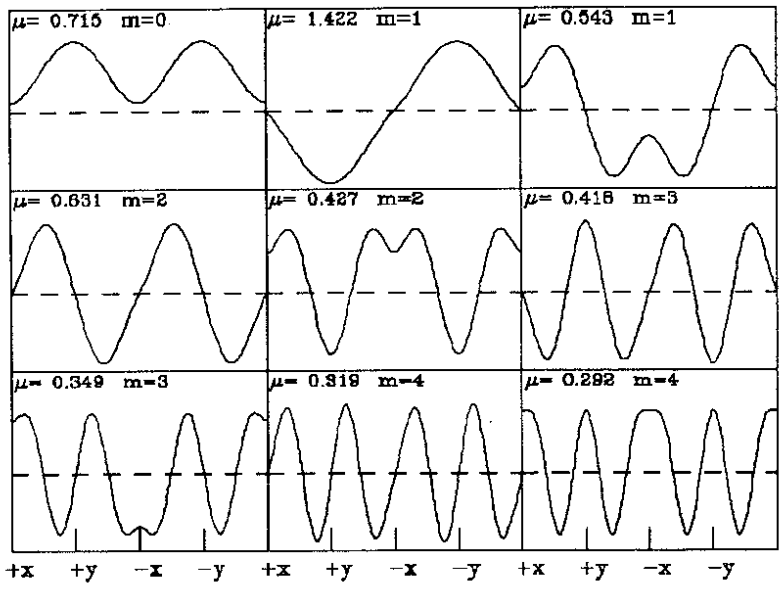

Figure 1: Eigenfunctions for an elliptic pipe with radius a/b=2. The horizontal axis is the circumference of the cross-section. The left edge corresponds to the positive x-axis and the first quarter point to the positive y-axis, etc., as indicated at the bottom. The eigenvalue (divided by b) and the mode identification are indicated at the top of each graph.

The dependence of the eigenvalue on the ellipticity is shown in Fig. 2. The left edge corresponds to the round pipe and the right edge two parallel plates. The cosine-like modes (including $m = 0$) are plotted in solid lines and the sine-like modes in dashed lines. One finds that the eigenvalues for lower sine-like modes increase rapidly as the ellipticity.

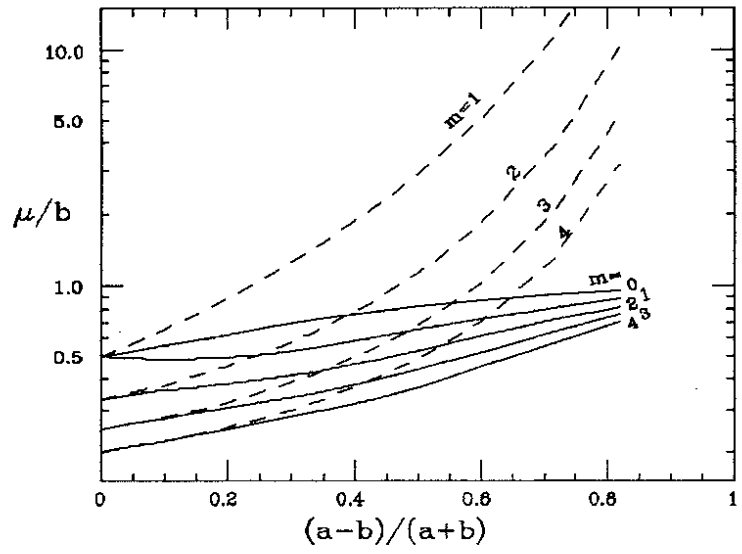

Figure 2: Eigenvalues (normalized by b) for elliptic pipes as a function of $(a-b)/(a+b)$. The solid lines are cosine-like modes and the dashed lins sine-like.

Time-dependence of the wake functions

Fig. 3 shows the longitudinal wake functions for $\boldsymbol{r}_s = \boldsymbol{r}_w = 0$ for three cases a/b=1, 2 and ∞ (b = 1cm). The horizontal axis is the normalized distance $\zeta = z/z_0$ with $z_0 = (b^2\rho_0)^{1/3}$ (= 17μm for copper). The long-range part is plotted with a magnified vertical scale on the right. The three cases have almost the same asymptotic behavior (the dotted line) but the approach to the asymptotic form is slower for flatter pipes, reflecting the larger eigenvalues of the sine-like modes.

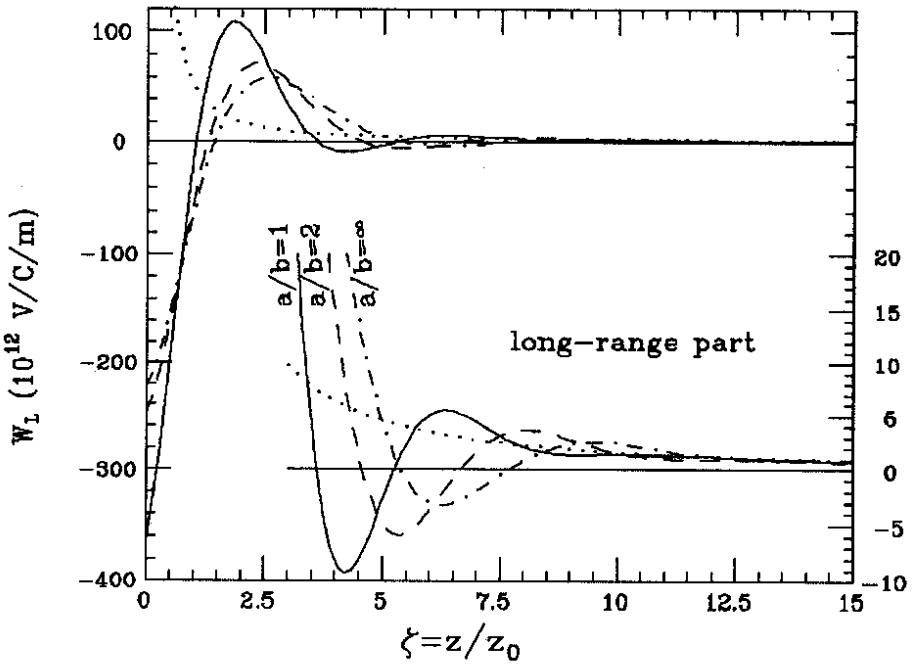

Figure 3: Longitudinal wake function for elliptic pipes with a/b=1, 2 and ∞.

Fig. 4 shows the transverse wake function near the center of elliptic pipes with b=1cm. The aspect ratio is a/b = 1, 1.2, 1.5, 2 and infinity as indicated in the figure. The four graphs are $\partial W_x/\partial x_s$, $\partial W_y/\partial y_s$, $\partial W_y/\partial y_w$ and $\partial W_y/\partial y_s + \partial W_y/\partial y_w$, in units of 10^{12} V/C/m^2. ($\partial W_x/\partial x_w$ is not plotted here.) The horizontal scale is the same as in Fig. 3. (Note that $\partial W_y/\partial y_w$ has different vertical scale). One finds that $\partial W_y/\partial y_s$ decreases as a/b increases but $\partial W_y/\partial y_w$, which vanishes for a round pipe, shows an opposite behavior. The sum $\partial W_y/\partial y_s + \partial W_y/\partial y_w$, which is the transverse wake when the source and the witness particles have the same displacement, is relatively insensitive to the aspect ratio if b is fixed.

Fig. 5 shows the transverse wake function for a hyperbolic pipe having a shape like the pole of a quadrupole magnet. The radius at the pole tip is b =1cm. (The area is cut at 2cm but the result is almost independent of the cut if it is larger than 1.5cm.) The horizontal scale is the same as in Fig. 3. The solid line is $\partial W_y/\partial y_s$ for the hyperbolic pipe. (Near the origin, $\boldsymbol{W}_\perp$ is parallel to $\boldsymbol{r}_s$ up to the first order of $\boldsymbol{r}_s$. The coefficient does not depend on the direction. Also note that $\boldsymbol{W}_\perp$ does not have the first order term of $\boldsymbol{r}_w$.) The dotted line is the asymptotic form ($\propto 1/\sqrt{z}$). The wake for the round pipe with radius 1cm is plotted in the dashed line for comparison. One finds the wake for the hyperbolic pipe is condiderably smaller than that for the round pipe in the short-range region but the difference is only slight in the asymptotic region.

The effects of the AC conductivity on the wake functions are shown in Fig. 6 (longitudinal wake) and Fig. 7(transverse) for round pipe and parallel plates with b=1cm. The assumed relaxation time is τ=8.1μm as in [3] so that $c\tau/z_0$=0.47. In all these graphs, the wake functions under DC conductivity are plotted in dashed lines for comparison. As was pointed out in [3], the AC conductivity makes the damping of the wake slower. The effect is less significant for parallel plates.

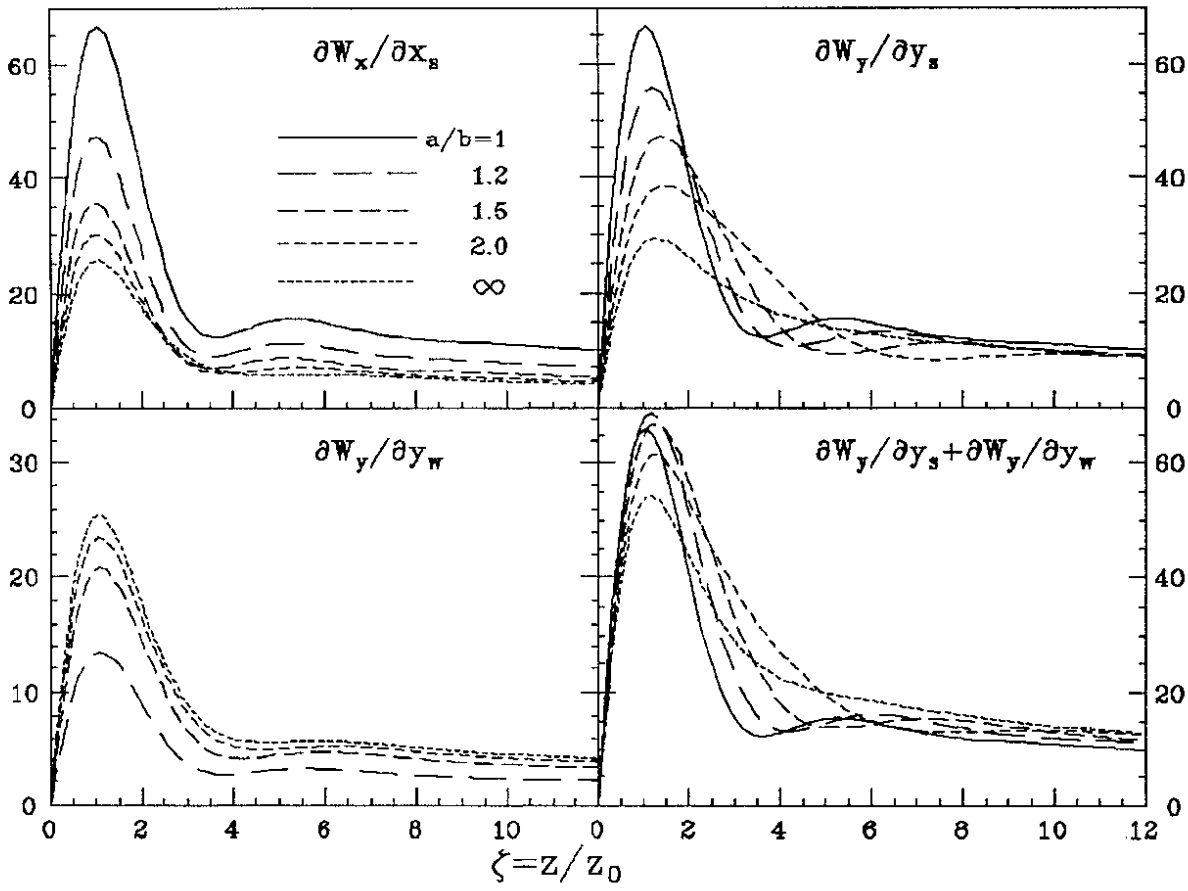

Figure 4: Transverse wake function for elliptic pipes with b=1cm.

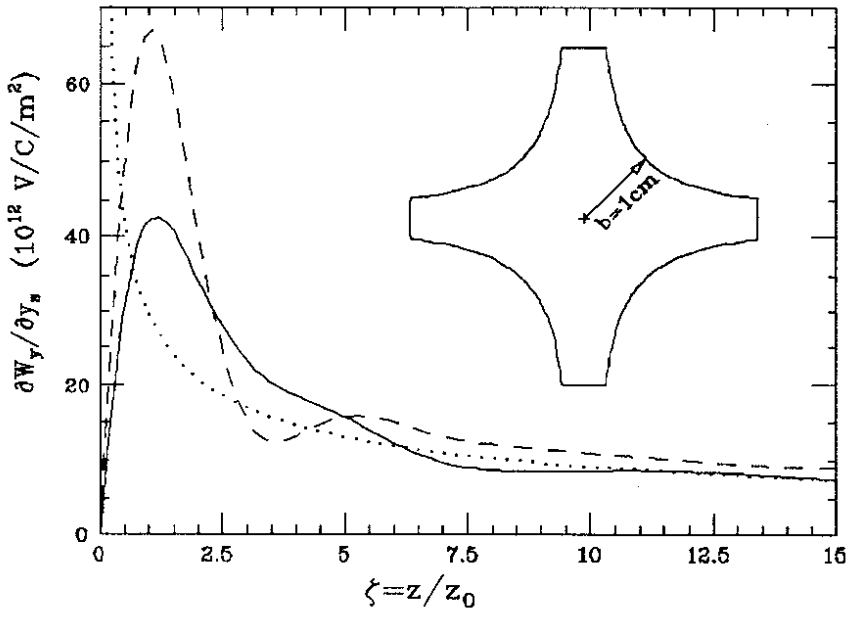

Figure 5: Transverse wake function (solid line) for a hyperbolic pipe with b=1cm. The dotted line is the asymptotic form and the dashed line is for the round pipe with radius 1cm.

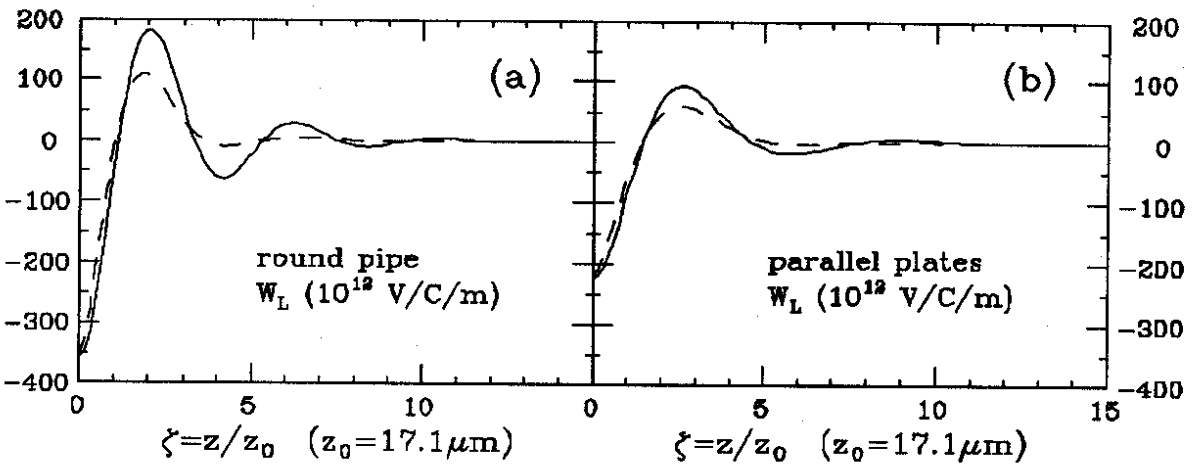

Figure 6: Longitudinal wake function with the AC conductivity taken into account. (a) round pipe and (b) parallel plates with b=1cm. The dashed lines are those with DC conductivity.

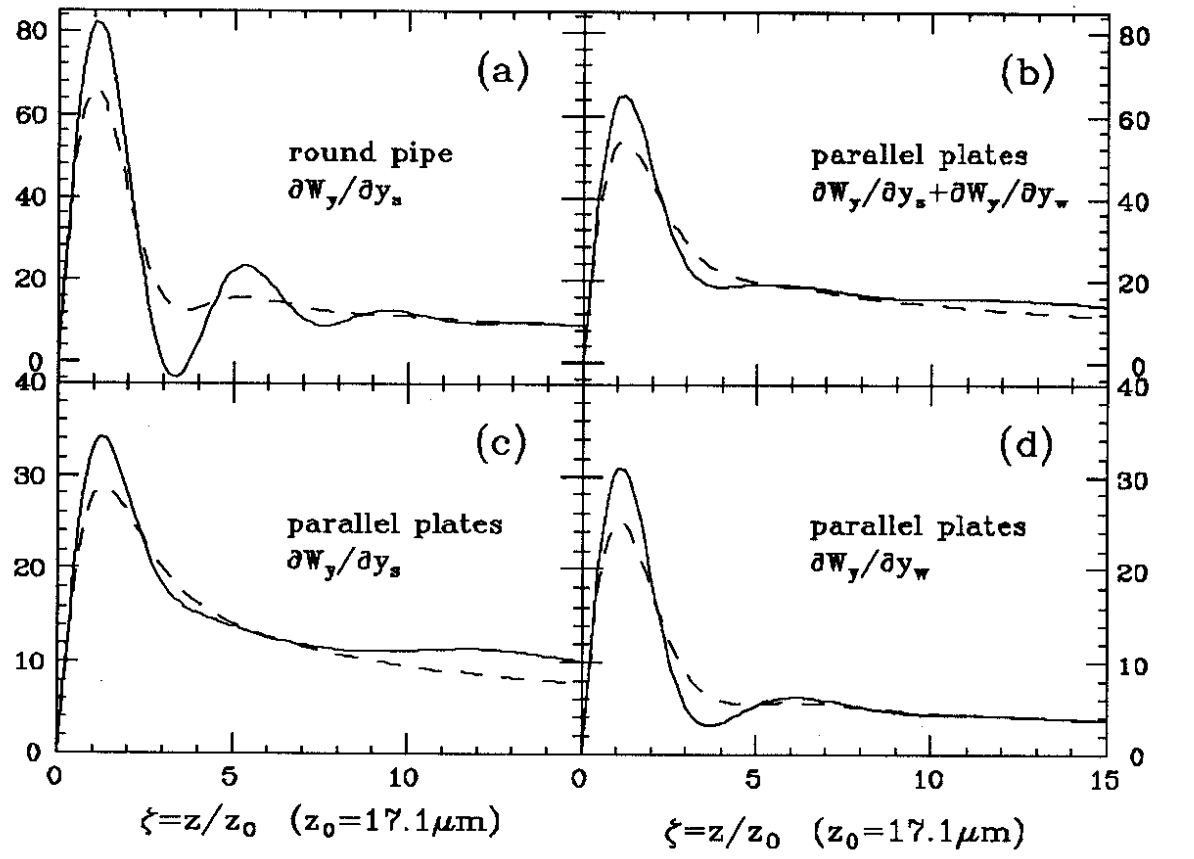

Figure 7: Transverse wake function with the AC conductivity taken into account for round pipe (a) and parallel plates (b,c,d) with b = 1cm. (a) and (c) are $\partial W_y/\partial y_s$, (b) is $\partial W_y/\partial y_s + \partial W_y/\partial y_w$ and (d) is $\partial W_y/\partial y_w$ in units of 10^{12} V/C/m^2. The dashed lines are those with DC conductivity.

Asymptotic form of the wake function

Next, we discuss the asymptotic form which is the most important in application. The asymptotic form of the longitudinal and transverse wake functions near the center of a round pipe of radius b are given by

$$W_L(z) = \frac{cZ_0\sqrt{\rho_0}}{4\pi\sqrt{\pi}b}\frac{1}{z^{3/2}} \tag{4.76}$$

$$\frac{\partial W_x}{\partial x_s} = \frac{cZ_0\sqrt{\rho_0}}{\pi\sqrt{\pi}b^3}\frac{1}{\sqrt{z}}. \tag{4.77}$$

At given $\boldsymbol{r}_s$ and $\boldsymbol{r}_w$ in the given beam pipe, the asymptotic form of the wake function is characterized by one parameter, i.e., the coefficient of $z^{-3/2}$ for W_L or that of $z^{-1/2}$ for the derivative of $\boldsymbol{W}_\perp$. In the following we shall normalize the coefficients by those for the round pipe.

Fig. 8 shows the asymptotic forms for elliptic and rectangular pipes as functions of $(a-b)/(a+b)$. One finds that the curves for W_L, $\partial W_x/\partial x_s$ and $\partial W_y/\partial y_s$ perfectly agree with those in Figures 1 and 2 in [6]. The aspect ratio a/b larger than ~ 2.5 gives practically the same results as the limit $a/b \to \infty$. The elliptic and rectangular pipes give almost the same wakes.

The curves for $\partial W_x/\partial x_w$ and $\partial W_y/\partial y_w$ are the contributions of the transverse shift of the witness particle, which are absent in the case of round pipes. (Actually, $\partial W_x/\partial x_w = -\partial W_y/\partial y_w$ always holds because E_z satisfies the Laplace equation.) The most interesting quantities when discussing the collimators and the final quads of linear colliders are the transverse force for $\boldsymbol{r}_s = \boldsymbol{r}_w$, i.e., $\partial W_x/\partial x_s + \partial W_x/\partial x_w$ and $\partial W_y/\partial y_s + \partial W_y/\partial y_w$. One sees that the vertical force for flat pipes is even larger, though slightly, than in the case of a round pipe tangent at the shorter radius. The ratio has been found to be $\pi^2/8 = 1.234$ in the limit of two parallel plates by Henke and Napoly [2]. One third of this value comes from $\partial W_y/\partial y_w$ and the rest from $\partial W_y/\partial y_s$. On the other hand, the horizontal force goes to zero when the aspect ratio becomes large. This is physically obvious. If the source and witness particles have the same horizontal displacement, there is no horizontal force in the limit $a/b \to \infty$ because of symmetry.

In the case of the hyperbolic pipe, the asymptotic form of the longitudinal wake is found to be slightly larger (by a factor 1.063) than that of the tangent round pipe and the transverse wake $\partial W_y/\partial y_s$ slightly smaller by a factor 0.835.

Dependence on the witness position

Next, let us discuss the dependence of the transverse asymptotic wake on the location of the witness particle when the source particle is exactly at the center of the pipe. The transverse wake is absent in the case of round pipes but this is not true in general.

The vertical asymptotic wake is plotted in Fig. 9 as a function of the vertical position of the witness particle y_w for rectangular and elliptic pipes. The aspect ratio is indicated by the line modes as shown in the figure with crosses for the curves for rectangular pipes. The vertical half aperture b is fixed in all cases. The wake W_y is normalized by $W_y^{(0)}$

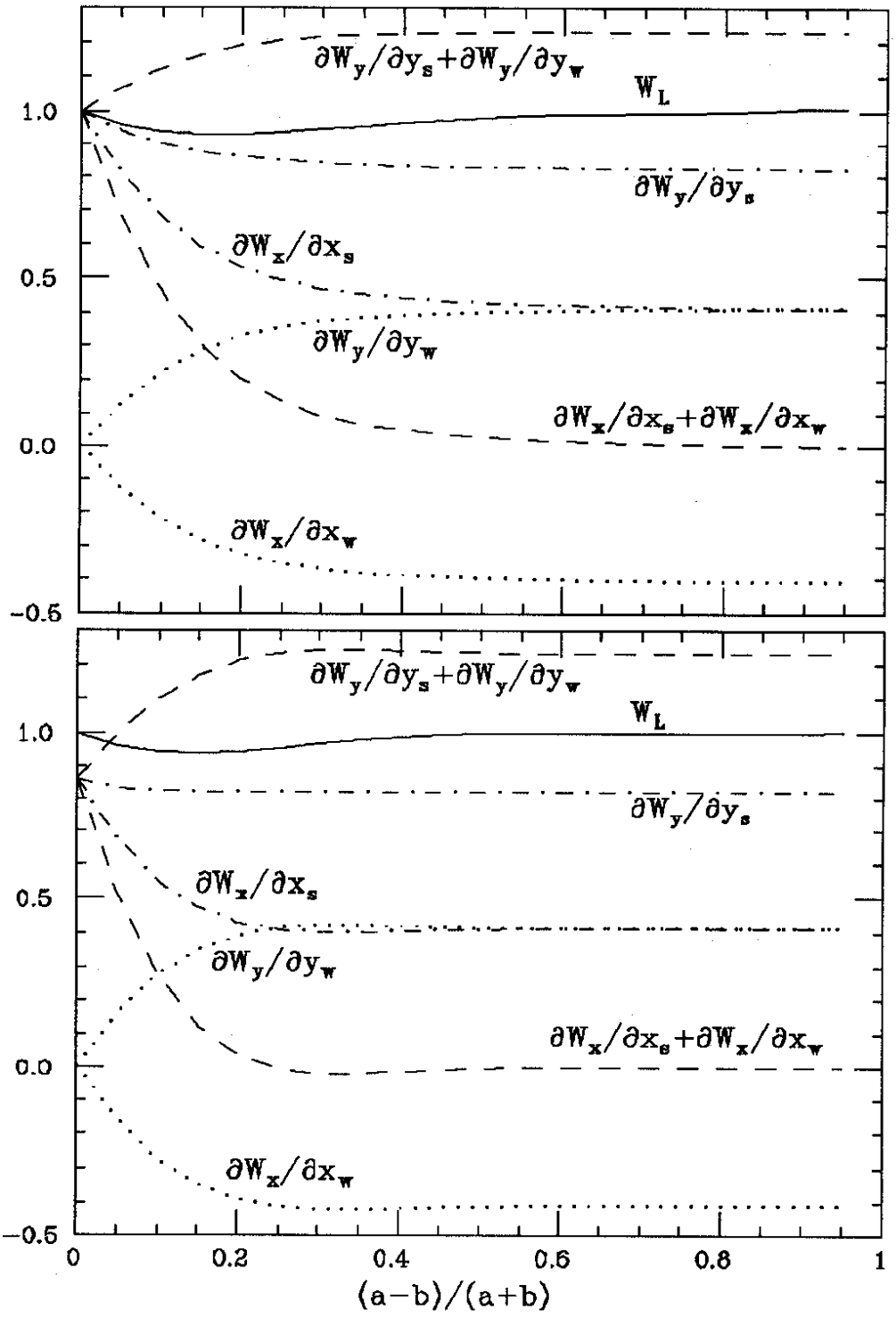

Figure 8: The coefficients of the asymptotic forms of the wake functions for elliptic pipes with the radii a and b (top) and for rectangular pipes with the width $2a$ and the height $2b$ (bottom) as functions of $(a-b)/(a+b)$. The values are normalized by those of the round pipe with radius b.

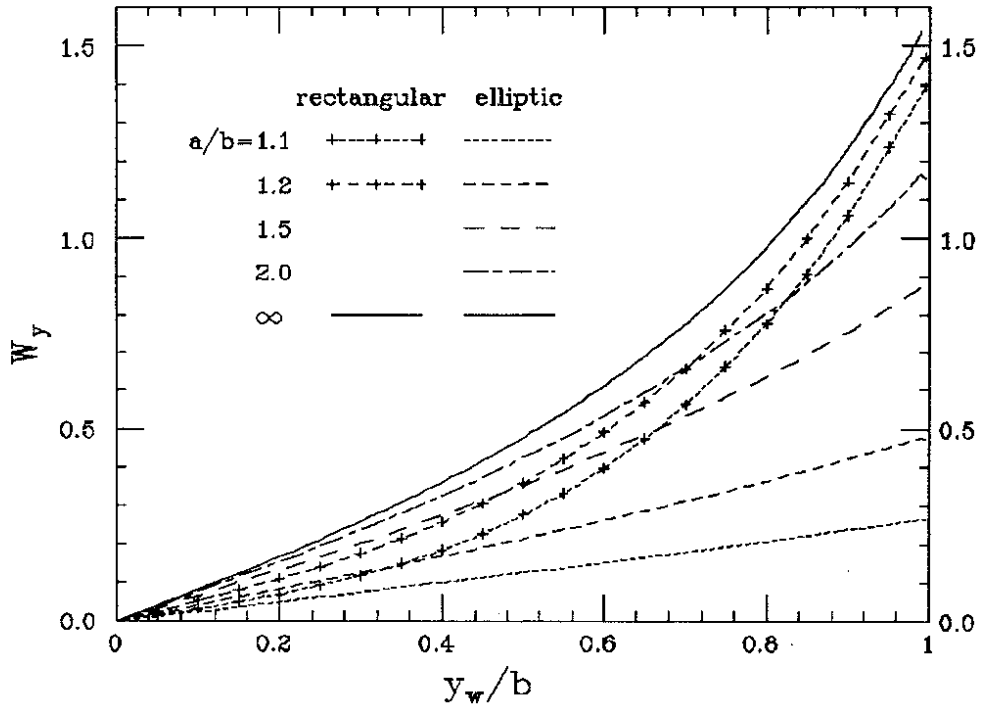

Figure 9: Vertical asymptotic wake vs. the location of the witness particle for rectangular and elliptic pipes of various aspect ratio with fixed vertical aperture.

defined by

$$W_y^{(0)} = b\left[\frac{\partial W_y}{\partial y_s}\right]_{\text{round pipe},\boldsymbol{r}_s=0} \tag{4.78}$$

which is the dipole wake for a round pipe when the source particle is near the pipe wall. From this figure we find the following facts. Firstly, W_y increases as y_w in rectangular pipes more rapidly than in elliptic pipes. Even for a small aspect ratio a/b=1.1, W_y is almost the same for $a/b = \infty$ when the witness particle is close to the wall. In the case of the elliptic pipes the wall curvature relaxes the concentration of the wall current and reduces the wake near the wall. Secondly, the y_w dependence is almost linear for elliptic pipes if $a/b \lesssim 1.5$ but W_y is still large near the wall unless a/b is extremely close to unity. For example, when a/b=1.2, W_y is about half of the dipole wake for a round pipe with $y_s = b$.

These facts strongly suggest that the collimator for linear colliders has to be round.

Fig. 10 is a similar plot for hyperbolic pipe. What is plotted is the transverse asymptotic wake for $\boldsymbol{r}_s = 0$ with the witness particle along the y-axis (W_y) and that along the 45-degree line (W_r). They are normalized by the same $W_y^{(0)}$ as in the previous plot.

Loss parameter for long bunches

Finally, let us confirm our computation of the loss parameter k_L for a long bunch, eq.(2.60), by comparing with the result by Piwinski [4,5]. Let us denote the distance

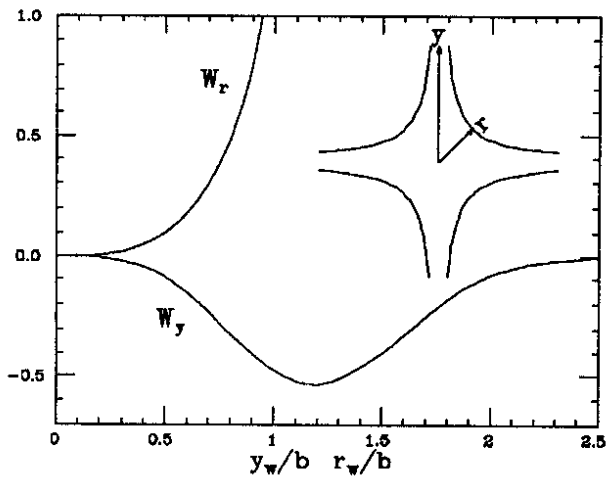

Figure 10: Transverse asymptotic wake for a hyperbolic pipe for $\boldsymbol{r}_w$ on the y-axis (W_y) and on the 45-degree line (W_r).

between the beam and the wall by $d = b - y_s$ ($0 \leq y_s \leq b$) and consider k_L as a function of d/b for fixed d. For the case of round pipes and two parallel plates, it has been shown by Piwinski that $k_{L(d/b=0)} = k_{L(d/b=1)}$ and that k_L has a weak minimum at $d/b = 2 - \sqrt{2}$ for round pipes and at $d/b = 0.6855$ for parallel plates. Fig. 11 shows $k_L(d, b)$ divided by $k_L(d, d)$ as a function of d/b. The solid line is for round pipes to be compared with Fig. 4a in [4], the dashed line for parallel plates with Fig. 2a in [5], and the dot-dashed line for elliptic pipes with $a/b = 1.5$. The first two curves perfectly agree with the results in [4,5]. One finds an elliptic pipe shows a qualitatively similar dependence as the other two cases, although $k_{L(d/b=0)} = k_{L(d/b=1)}$ does not hold exactly.

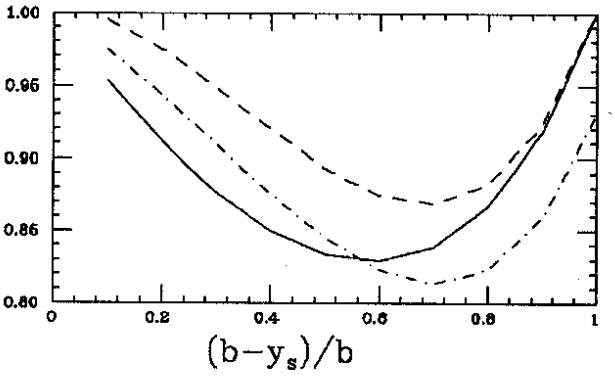

Figure 11: Loss parameter k_L for long bunch with fixed distance $d = b - y_s$ between the beam and the wall. The horizontal axis is d divided by the half aperture b of the pipe. The loss parameter is normalized by that for the beam at the center of a round pipe with radius $b = d$.

5 Summary

We have developed a method of computing the resistive wall impedance/wake function for arbitrary shapes of the pipe crosssection under the conditions that (a) the particle is ultrarelativistic, (b) the pipe is longitudinally uniform, and (c) the skin depth is smaller than the typical dimension of the pipe (and than the thickness of the wall material). The location of the source and witness particles is arbitrary and the short-range effects due to the reduced phase velocity and to the AC conductivity can be included. In our

method, the Maxwell equation is solved by using the boundary element method, which is basically the discretization of the Kirchhoff integral equation. The computer code is very powerful and is more convenient, except for the round pipe case, than analytic formulas, even if available.

Among our assumptions, (a) can be relaxed relatively easily by using the Helmholz equation instead of the Laplace equation. However, (b) is very hard to remove. For the impedance calculation of resistive and non-uniform pipes, one has to be satisfied with the simple sum of the geometric impedance and the integral of the resistive impedance with the assumption of the smooth change of the wall. A related problem is the propagation of the wave in pipes of finite length. Usually, the generated high-frequency wave can interact with the particle only after travelling over a distance which is typically kL^2. In the case of the final quad in linear colliders ($1/k \sim 100\mu$m, $L \sim 1$cm), this distance is about 1m which can not be ignored. Further investigation is needed for these extreme problems.

A The self-adjointness of the operators

We prove here that the operators $\mathcal{G}^{-1}\mathcal{D}$ and $\mathcal{M}$ are self-adjoint.

We denote the kernel function of an operator $\mathcal{A}$ by Kern$[\mathcal{A}]$, i.e.,

$$(\mathcal{A}f)(s) = \oint ds' \,\mathrm{Kern}[\mathcal{A}](s,s')f(s'). \tag{A.79}$$

Obviously, the self-adjointness of $\mathcal{A}$, $\mathcal{A}^\dagger = \mathcal{A}$, is equivalent to the symmetry of Kern$[\mathcal{A}]$: Kern$[\mathcal{A}](s,s')$=Kern$[\mathcal{A}](s',s)^*$. The asterisk denotes complex conjugate, but it is actually not needed because we treat only real kernels.

The kernel for the product of two operators is given by the convolution of the two kernels;

$$\mathrm{Kern}[\mathcal{A}\mathcal{B}](s,s') = \oint ds' \,\mathrm{Kern}[\mathcal{A}](s,s'')\mathrm{Kern}[\mathcal{B}](s'',s'). \tag{A.80}$$

First, let us discuss the self-adjointness of $\mathcal{G}^{-1}\mathcal{D}$, which is equivalent to $\mathcal{G}\mathcal{D}^\dagger = \mathcal{D}\mathcal{G}^\dagger$.

It is obvious that $\mathcal{G}$ is self-adjoint, i.e., $\mathcal{G}^\dagger = \mathcal{G}$, because $G(\boldsymbol{r},\boldsymbol{r}') = G(\boldsymbol{r}',\boldsymbol{r})$. By the definition of the operator $\mathcal{D}$, we have

$$\mathrm{Kern}[\mathcal{D}^\dagger](s,s') = \delta(s-s') + \boldsymbol{n}\cdot\nabla_\perp G(\boldsymbol{r},\boldsymbol{r}'). \tag{A.81}$$

Therefore,

$$\begin{aligned}
\mathrm{Kern}[\mathcal{G}\mathcal{D}^\dagger](s,s') &= G(\boldsymbol{r},\boldsymbol{r}') + \oint ds'' G(\boldsymbol{r},\boldsymbol{r}'')\left[\boldsymbol{n}''\cdot\nabla''_\perp G(\boldsymbol{r}'',\boldsymbol{r}')\right], \\
\mathrm{Kern}[\mathcal{D}\mathcal{G}^\dagger](s,s') &= G(\boldsymbol{r},\boldsymbol{r}') + \oint ds'' \left[\boldsymbol{n}''\cdot\nabla''_\perp G(\boldsymbol{r},\boldsymbol{r}'')\right] G(\boldsymbol{r}'',\boldsymbol{r}'),
\end{aligned} \tag{A.82}$$

from which we obtain

$$\begin{aligned}
\mathrm{Kern}[\mathcal{G}\mathcal{D}^\dagger - \mathcal{D}\mathcal{G}^\dagger] &= \oint ds'' \boldsymbol{n}'' \cdot [G(\boldsymbol{r},\boldsymbol{r}'')\nabla''_\perp G(\boldsymbol{r}'',\boldsymbol{r}') - \nabla''_\perp G(\boldsymbol{r},\boldsymbol{r}'')G(\boldsymbol{r}'',\boldsymbol{r}')] \\
&= \int_\Omega d\boldsymbol{r}''\nabla''_\perp \cdot [G(\boldsymbol{r},\boldsymbol{r}'')\nabla''_\perp G(\boldsymbol{r}'',\boldsymbol{r}') - \nabla''_\perp G(\boldsymbol{r},\boldsymbol{r}'')G(\boldsymbol{r}'',\boldsymbol{r}')] \\
&= \int_\Omega d\boldsymbol{r}'' [G(\boldsymbol{r},\boldsymbol{r}'')\Delta''_\perp G(\boldsymbol{r}'',\boldsymbol{r}') - \Delta''_\perp G(\boldsymbol{r},\boldsymbol{r}'')G(\boldsymbol{r}'',\boldsymbol{r}')] \\
&= \int_\Omega d\boldsymbol{r}'' [-G(\boldsymbol{r},\boldsymbol{r}'')\delta(\boldsymbol{r}''-\boldsymbol{r}') + \delta(\boldsymbol{r}-\boldsymbol{r}'')G(\boldsymbol{r}'',\boldsymbol{r}')] \\
&= 0,
\end{aligned}$$

where $\int_\Omega d\boldsymbol{r}''$ is the integral over the crossection Ω. We have made use of the fact that $G(\boldsymbol{r},\boldsymbol{r}')$ satisfies the Laplace equation (2.6). Thus, $\mathcal{G}^{-1}\mathcal{D}$ is self-adjoint.

Next, let us discuss $\mathcal{M}$. Eqs.(2.15) and (2.16) can be written in the form

$$\begin{pmatrix} \mathcal{N} & \mathcal{T} \\ -\mathcal{T} & \mathcal{N} \end{pmatrix} \begin{pmatrix} |E_n\rangle \\ -|E_\tau\rangle \end{pmatrix} = -ik \begin{pmatrix} \mathcal{C} & \mathcal{S} \\ -\mathcal{S} & \mathcal{C} \end{pmatrix} \begin{pmatrix} |E_z\rangle \\ |Z_0 H_z\rangle \end{pmatrix}. \tag{A.83}$$

The upper left component of the operator

$$\begin{pmatrix} \mathcal{C} & \mathcal{S} \\ -\mathcal{S} & \mathcal{C} \end{pmatrix}^{-1} \begin{pmatrix} \mathcal{N} & \mathcal{T} \\ -\mathcal{T} & \mathcal{N} \end{pmatrix} \tag{A.84}$$

is equal to $\mathcal{M}^{-1}$. Therefore, it is sufficient to prove the self-adjointness of the above operator, or, equivalently, of the operator

$$\begin{pmatrix} \mathcal{N} & \mathcal{T} \\ -\mathcal{T} & \mathcal{N} \end{pmatrix} \begin{pmatrix} \mathcal{C} & \mathcal{S} \\ -\mathcal{S} & \mathcal{C} \end{pmatrix}^\dagger. \tag{A.85}$$

Since it is obvious by definition that $\mathcal{C}^\dagger = \mathcal{C}$ and $\mathcal{S}^\dagger = -\mathcal{S}$, it suffices to prove

$$(\mathcal{N} + i\mathcal{T})(\mathcal{C} + i\mathcal{S}) = (\mathcal{C} + i\mathcal{S})(\mathcal{N}^\dagger - i\mathcal{T}^\dagger). \tag{A.86}$$

Since

$$\begin{aligned}
\mathrm{Kern}[\mathcal{C} + i\mathcal{S}] &= (\boldsymbol{n} + i\boldsymbol{\tau}) \cdot \boldsymbol{n}' G(s,s') = (\boldsymbol{n}' - i\boldsymbol{\tau}') \cdot \boldsymbol{n}\, G(s,s') \\
\mathrm{Kern}[\mathcal{N} + i\mathcal{T}] &= \delta(s-s') + (\boldsymbol{n} + i\boldsymbol{\tau}) \cdot \nabla'_\perp G(s,s'), \\
\mathrm{Kern}[\mathcal{N}^\dagger - i\mathcal{T}^\dagger] &= \delta(s-s') + (\boldsymbol{n}' - i\boldsymbol{\tau}') \cdot \nabla_\perp G(s,s'),
\end{aligned} \tag{A.87}$$

we find

$$\begin{aligned}
&\mathrm{Kern}[(\mathcal{N} + i\mathcal{T})(\mathcal{C} + i\mathcal{S}) - (\mathcal{C} + i\mathcal{S})(\mathcal{N}^\dagger - i\mathcal{T}^\dagger)] \qquad \text{(A.88)} \\
&= \oint ds''[\boldsymbol{v} \cdot \nabla''_\perp G(s,s'')\boldsymbol{v}'^* \cdot \boldsymbol{n}'' G(s'',s') - \boldsymbol{v} \cdot \boldsymbol{n}'' G(s,s'')\boldsymbol{v}'^* \cdot \nabla''_\perp G(s'',s')] \\
&= \oint ds'' \boldsymbol{n}'' \cdot [\boldsymbol{v} \cdot \nabla''_\perp G(s,s'')\boldsymbol{v}'^* G(s'',s') - \boldsymbol{v} G(s,s'')\boldsymbol{v}'^* \cdot \nabla''_\perp G(s'',s')] \\
&= \oint d\boldsymbol{r}''\nabla''_\perp \cdot [\boldsymbol{v} \cdot \nabla''_\perp G(s,s'')\boldsymbol{v}'^* G(s'',s') - \boldsymbol{v} G(s,s'')\boldsymbol{v}'^* \cdot \nabla''_\perp G(s'',s')] \\
&= \oint d\boldsymbol{r}'' \sum_{i,j=x,y} v_i v_j^* [\partial''_i \partial''_j G(s,s'') \cdot G(s'',s') - G(s,s'')\partial''_i \partial''_j G(s'',s')],
\end{aligned}$$

where $\boldsymbol{v} = \boldsymbol{n} + i\boldsymbol{\tau}$. Since $v_y = n_y + i\tau_y = -\tau_x + in_x = iv_x$, $v_x v_y'^*$ and $v_y v_x'^*$ cancell each other and $v_y v_y'^* = v_x v_x'^* = \boldsymbol{v} \cdot \boldsymbol{n}'$. Thus, we find the above expression is equal to

$$\oint d\boldsymbol{r}'' \boldsymbol{v} \cdot \boldsymbol{n}' [\Delta_\perp'' G(s, s'') \cdot G(s'', s) - G(s, s'') \Delta_\perp'' G(s'', s')] = 0. \tag{A.89}$$

Thus, $\mathcal{M}$ is self-adjoint.

B Basic Wake Functions

Basic wake functions f_L and f_T

We define the dimensionless functions $f_L(\zeta)$ and $f_T(\zeta)$ as

$$f_L(\zeta) = \frac{-1}{4\pi} \int_{-\infty}^{+\infty} d\omega e^{-i\omega\zeta} \frac{e^{\mp \pi i/4} (\pm\omega)^{1/2}}{1 - \frac{1}{2} e^{\pm \pi i/4} (\pm\omega)^{3/2}}, \tag{B.90}$$

$$f_T(\zeta) = \frac{1}{4\pi} \int_{-\infty}^{+\infty} d\omega e^{-i\omega\zeta} \frac{e^{\pm \pi i/4} (\pm\omega)^{-1/2}}{1 - \frac{1}{2} e^{\pm \pi i/4} (\pm\omega)^{3/2}}, \tag{B.91}$$

where $\pm$ is the sign of ω. They have the relation

$$f_T(\zeta) = \int_\zeta^{+\infty} f_L(\zeta) d\zeta. \tag{B.92}$$

The normalization is chosen such that $f_L(0_+) = -1$. These functions are plotted in Fig. 12 together with the asymptotic forms for large ζ

$$f_L(\zeta) \approx \frac{1}{4\sqrt{\pi}\zeta^{3/2}}, \tag{B.93}$$

$$f_T(\zeta) \approx \frac{1}{2\sqrt{\pi\zeta}}. \tag{B.94}$$

As can be seen in this figure, the approach to the asymptotic forms is fairly slow. The deviation is sizable even at $\zeta \sim 9$ (longitudinal) and ~ 4 (transverse). For the transverse function, however, we may in practice use the asymptotic form down to a much smaller value of ζ, say ~ 1, because of the following accidental relation

$$\int_0^\infty \left[f_T(\zeta) - \frac{1}{2\sqrt{\pi\zeta}} \right] d\zeta = 0. \tag{B.95}$$

The longitudinal and the transverse (per unit displacement of the source particle) wake functions for a round pipe with radius a per unit pipe length are given by

$$W_L(z) = \frac{cZ_0}{\pi a^2} f_L(z/z_1), \tag{B.96}$$

$$\frac{\partial W_y}{\partial y_s}(z) = \frac{cZ_0}{\pi a^4} 2z_1 f_T(z/z_1), \qquad z_1 = (a^2\rho_0)^{1/3}. \tag{B.97}$$

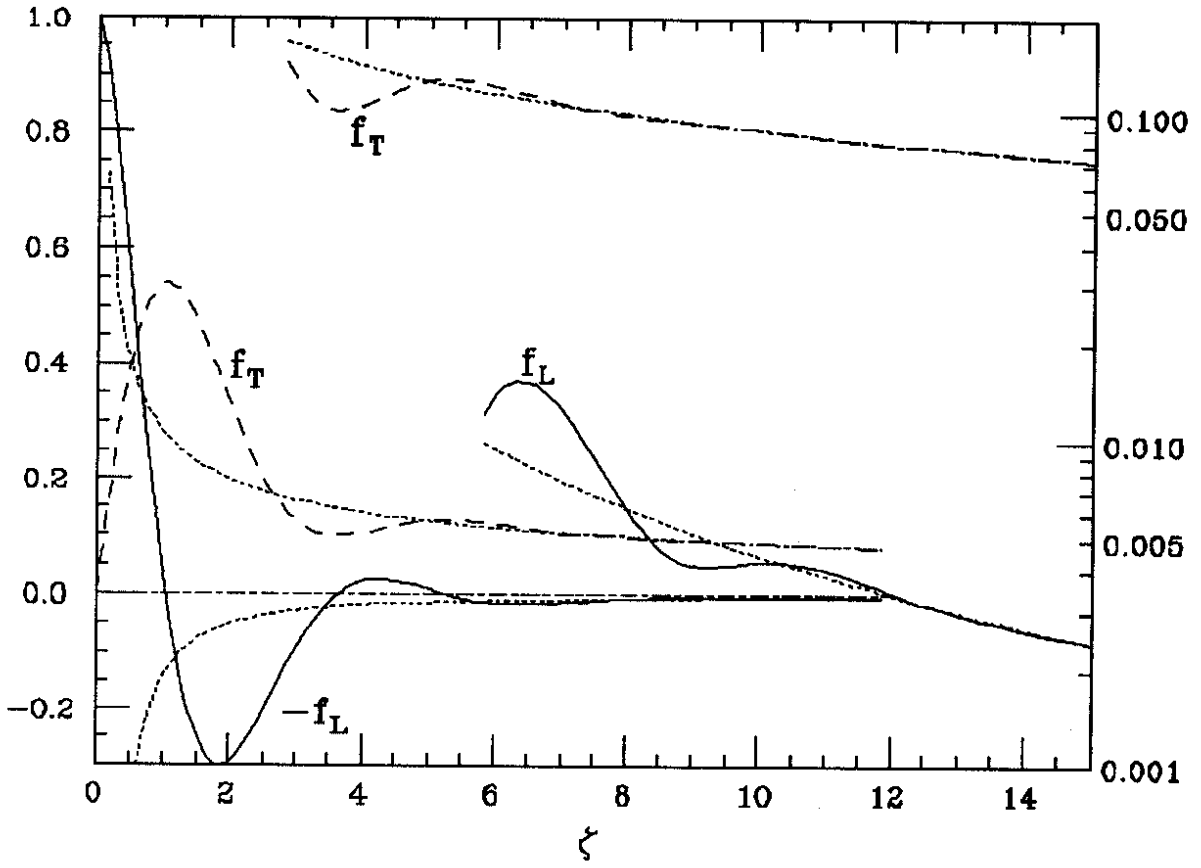

Figure 12: The basic wake functions f_L (solid) and f_T (dashed) and their asymptotic forms (dotted) defined in eqs.(B.93) and (B.94). The large ζ region is plotted in logarithmic scale too (scale on the right).

The Taylor expansions at the origin are

$$f_L(\zeta) = -\sum_{n=0}^{\infty} \frac{(-1)^n 2^n}{\Gamma(3n/2+1)} \zeta^{3n/2} \qquad (0 \le \zeta < \infty) \tag{B.98}$$

$$f_T(\zeta) = \sum_{n=0}^{\infty} \frac{(-1)^n 2^{n+1}}{\Gamma(3n/2+2)} \zeta^{3n/2+1} \qquad (0 \le \zeta < \infty). \tag{B.99}$$

For large ζ, we have asymptotic expansions

$$f_L(\zeta) = -\frac{4}{3} e^{-2^{-1/3}\zeta} \cos\left(\frac{\sqrt{3}}{2^{1/3}}\zeta\right) + \frac{1}{4\sqrt{\pi}\zeta^{3/2}} \left[1 + \sum_{n=1}^{\infty} \frac{(-1)^n \Gamma(3n+3/2)}{\Gamma(3/2) 4^n \zeta^{3n}}\right] \tag{B.100}$$

$$f_T(\zeta) = -\frac{2^{4/3}}{3} e^{-2^{-1/3}\zeta} \cos\left(\frac{\sqrt{3}}{2^{1/3}}\zeta + \frac{\pi}{3}\right) + \frac{1}{2\sqrt{\pi\zeta}} \left[1 + \sum_{n=1}^{\infty} \frac{(-1)^n \Gamma(3n+1/2)}{\Gamma(1/2) 4^n \zeta^{3n}}\right], \tag{B.101}$$

although they do not converge. The series in the square brackets can be rewritten in the form of continued fractions like

$$\cfrac{1}{1 + \cfrac{c_1 \zeta^{-3}}{1 + \cfrac{c_2 \zeta^{-3}}{1 + \ldots}}}. \tag{B.102}$$

The coefficients c_1, c_2, $\cdots$ cannot be expressed in analytic forms but can be computed numerically. These continued fractions converge and, together with the Taylor expansions (B.98) and (B.99), allow one to compute $f_L(\zeta)$ and $f_T(\zeta)$ for any ζ.

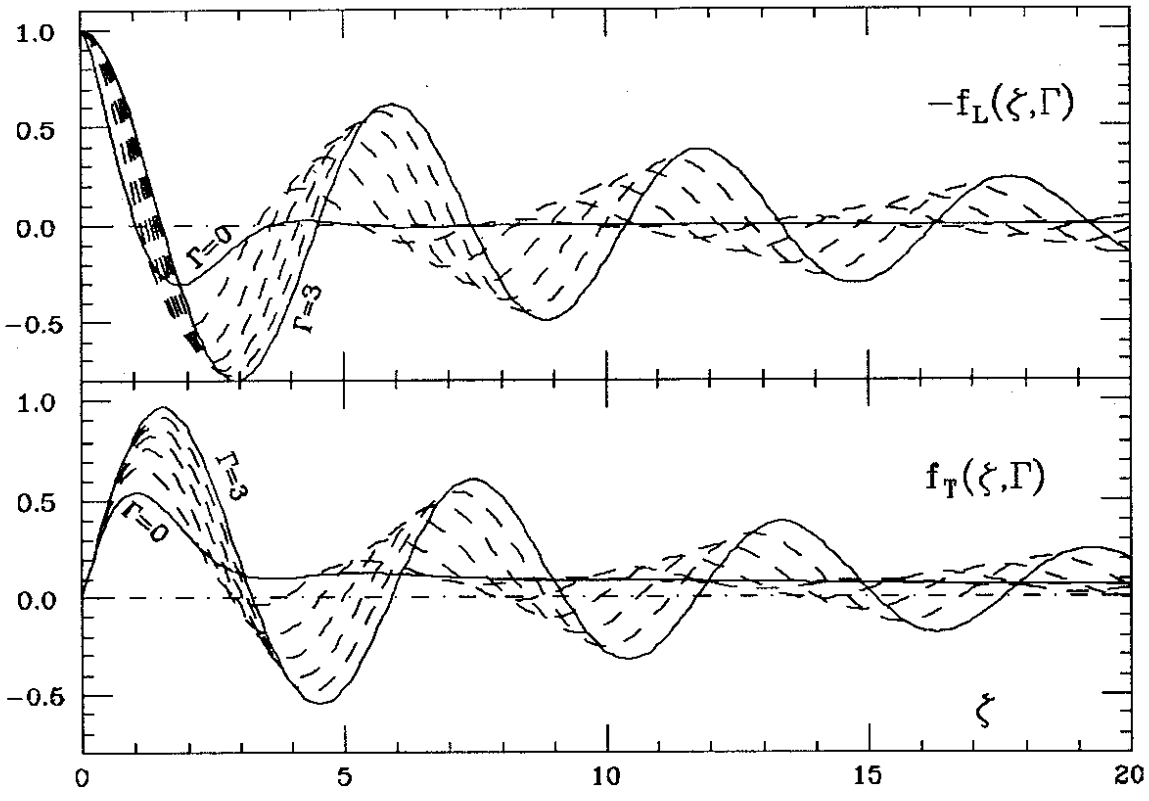

Figure 13: The functions $f_L(\zeta,\Gamma)$ (top) and $f_T(\zeta,\Gamma)$ (bottom) as functions of ζ for Γ=0 and 3 (solid lines) and for the values in between with step 0.5 (dashed lines).

Wake functions under AC conductivity

The basic wake functions with AC conductivity are denoted by $f_L(\zeta,\Gamma)$ and $f_T(\zeta,\Gamma)$. They are defined by eqs.(B.90) and (B.91) with '1' in the denominator replaced with $(1 \mp i\Gamma\omega)^{-1/2}$. An integral representation more convenient for numerical integration is found by changing the integration contour to the imaginary axis. The result is

$$f_T(\zeta,\Gamma) = -\Re\frac{1}{c_0(1+c_0^3/16)}e^{-c_0\zeta} + \frac{1}{\pi}\int_0^\infty dy \frac{(1+\Gamma y^2)^2}{(1+\Gamma y^2)^4 + y^6/4} e^{-\zeta y^2/(1+\Gamma y^2)}, \quad \text{(B.103)}$$

where c_0 is the complex root of the quartic equation $\Gamma c_0^4 - c_0^3 - 4 = 0$ in the first quadrant and is given explicitly by

$$c_0 = 2^{1/3}\frac{1+i\sqrt{1+c_1^{-3/2}}}{\sqrt{c_1}(1+\frac{1}{2}c_1^{-3/2})} \quad \text{(B.104)}$$

with

$$c_1 = \frac{1}{2}[(\sqrt{1+\Gamma_1^3}+1)^{1/3} - (\sqrt{1+\Gamma_1^3}-1)^{1/3}], \qquad (\Gamma_1 = 2^{10/3}\Gamma/3)$$

$$= \left[\Gamma_1 + (1+\sqrt{1+\Gamma_1^3})^{2/3} + \Gamma_1^2(1+\sqrt{1+\Gamma_1^3})^{-2/3}\right]^{-1}. \qquad \text{(B.105)}$$

The expressions for $f_L(\zeta,\Gamma)$ are easily found from the relation $f_L = -df_T/d\zeta$.

Loss parameter function g_L

The basic function g_L for the loss parameter of Gaussian bunches is defined by

$$g_L(\sigma) = \frac{1}{2\pi}\int_{-\infty}^{+\infty} d\omega e^{-\sigma^2\omega^2} \frac{e^{\mp\pi i/4}(\pm\omega)^{1/2}}{1-\frac{1}{2}e^{\pm\pi i/4}(\pm\omega)^{3/2}} = -\int_0^\infty f_L(\zeta)\frac{\exp(-\zeta^2/4\sigma^2)}{\sqrt{\pi}\sigma}d\zeta. \qquad \text{(B.106)}$$

It is normalized as $g_L(0) = 1$ and has the asymptotic form for large σ

$$g_L(\sigma) \approx \frac{\Gamma(3/4)}{2\sqrt{2}\pi}\frac{1}{\sigma^{3/2}}, \qquad (\sigma \gg 1). \qquad \text{(B.107)}$$

The function g_L is plotted in Fig. 14 by the solid line together with the asymptotic form (B.107) by the dashed line. One finds that the asymptotic form can be used even down to $\sigma \sim 1$. The Taylor expansion and the asymptotic expansion are

$$g_L(\sigma) = \sum_{n=0}^{\infty}\frac{(-2)^n}{\Gamma(3n/4+1)}\sigma^{3n/2} = \sum_{n=1}^{\infty}\sin\frac{n\pi}{4}\Gamma\left(\frac{3n}{4}\right)\frac{1}{2^n}\sigma^{-3n/2}. \qquad \text{(B.108)}$$

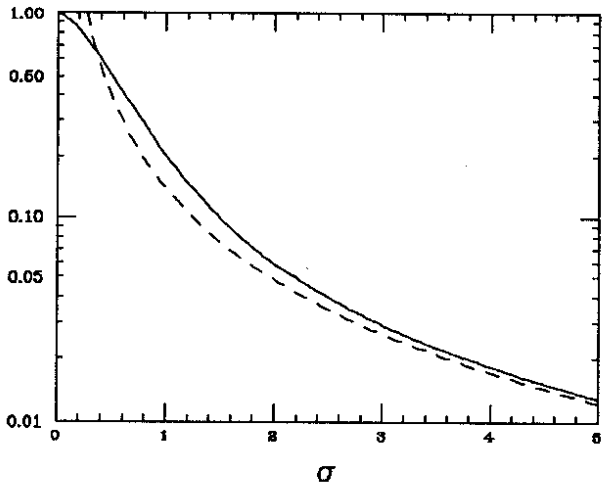

Figure 14: Function $g_L(\sigma)$ (solid line) and its asymptotic form (dashed line) given in eq.(B.107).

References

[1] N. Merminga, J. Irwin, R. Helm and R. D. Ruth, proc. IEEE Part. Acc. Conf. May 6-9, 1991, San Francisco, CA, page 219.
J. Irwin, D. Helm, N. Merminga and R. Nelson, *A Final Focus System for the Next Linear Collider*, to be published in XVth International Conf. on High Energy Acc. , July 20-24, 1992, Hamburg.

[2] H. Henke and O. Napoly, Proc. 2nd European Acc. Conf., June 12-16, 1990, Nice, France, page 1046. Also, CERN-LEP-RF 89-71, 1989, Geneva, Switzerland.

[3] K. Bane, *The Short Range Resistive Wall Wakefields*, SLAC-AP-87, June 1991.

[4] A. Piwinski, *Wake Fields and Ohmic Losses in Round Vacuum Chambers*, DESY, HERA 92-11, Jan. 1992, Hamburg.

[5] A. Piwinski, *Wake Fields and Ohmic Losses in Flat Vacuum Chambers*, DESY, HERA 92-04, May 1992, Hamburg.

[6] R. L. Gluckstern, J. van Zeijts and B. Zotter, *Coupling Impedance of Beam Pipes of General Cross Section*, CERN SL/AP 92-25, 18 June 1992, Geneva.

[7] J. D. Jackson, *Classical Electrodynamics*, John Wiley & Sons, New York, 1974, page 432.